

Communication

Optoelectronic Simulations of InGaN-Based Green Micro-Resonant Cavity Light-Emitting Diodes with Staggered Multiple Quantum Wells

Tsau-Hua Hsieh ^{1,2,†}, Wei-Ta Huang ^{3,4,†} , Kuo-Bin Hong ⁴, Tzu-Yi Lee ³, Yi-Hong Bai ³, Yi-Hua Pai ³, Chang-Ching Tu ⁴, Chun-Hui Huang ², Yiming Li ¹  and Hao-Chung Kuo ^{3,4,*} 

¹ Department of Electrical and Computer Engineering, Institute of Communications Engineering, National Yang Ming Chiao Tung University, Hsinchu 30010, Taiwan

² Technology Development Center, InnoLux Corporation, Hsinchu 35053, Taiwan

³ Department of Photonics, Institute of Electro-Optical Engineering, College of Electrical and Computer Engineering, National Yang Ming Chiao Tung University, Hsinchu 30010, Taiwan

⁴ Semiconductor Research Center, Hon Hai Research Institute, Taipei 11492, Taiwan

* Correspondence: hckuo0206@nycu.edu.tw

† These authors contributed equally to this work.

Abstract: In this research, we compared the performance of commercial μ -LEDs and three-layered staggered QW μ -LED arrays. We also investigated the self-heating effect. We proposed a green micro-resonant cavity light-emitting diode (μ -RCLED) that consists of a three-layer staggered InGaN with multiple quantum wells (MQWs), a bottom layer of nanoporous n-GaN distributed Bragg reflectors (DBRs), and a top layer of Ta₂O₅/SiO₂ DBRs. We systematically performed simulations of the proposed μ -RCLEDs. For the InGaN MQWs with an input current of 300 mA, the calculated wavefunction overlaps are 8.8% and 18.1% for the regular and staggered structures, respectively. Furthermore, the staggered MQWs can reduce the blue-shift of electroluminescence from 10.25 nm, obtained with regular MQWs, to 2.25 nm. Due to less blue-shift, the output power can be maintained even at a high input current. Conversely, by employing 6.5 pairs of Ta₂O₅/SiO₂ DBRs stacks, the full width at half maximum (FWHM) can be significantly reduced from 40 nm, obtained with ordinary μ -LEDs, to 0.3 nm, and a divergence angle smaller than 60° can be obtained. Our simulation results suggest that the μ -RCLEDs can effectively resolve the wavelength instability and color purity issues of conventional μ -LEDs.

Keywords: InGaN; light-emitting diode; resonant cavity; nanoporous DBR; micro-LED



Citation: Hsieh, T.-H.; Huang, W.-T.; Hong, K.-B.; Lee, T.-Y.; Bai, Y.-H.; Pai, Y.-H.; Tu, C.-C.; Huang, C.-H.; Li, Y.; Kuo, H.-C. Optoelectronic Simulations of InGaN-Based Green Micro-Resonant Cavity Light-Emitting Diodes with Staggered Multiple Quantum Wells. *Crystals* **2023**, *13*, 572. <https://doi.org/10.3390/cryst13040572>

Academic Editors: Daisuke Iida and Zhe Zhuang

Received: 3 March 2023

Revised: 24 March 2023

Accepted: 26 March 2023

Published: 27 March 2023



Copyright: © 2023 by the authors. Licensee MDPI, Basel, Switzerland. This article is an open access article distributed under the terms and conditions of the Creative Commons Attribution (CC BY) license (<https://creativecommons.org/licenses/by/4.0/>).

1. Introduction

InGaN-based light-emitting diodes (LEDs) are currently being considered a viable solution for a range of applications, such as light fidelity (Li-Fi) [1,2], underwater optical communication (UWOC) [3], smart displaying signboards [4], and indoor positioning [5]. This is due to their low power consumption, long lifespan, high brightness, and superior contrast [1,2,6]. The widespread use of LEDs in everyday life makes them an ideal platform for visible light communication (VLC) and LED-based displays. Compared to laser diodes, LEDs are more cost-effective and easier to manufacture. However, additional processing steps are necessary for creating the active region responsible for stimulated emission in lasers [7].

For display applications, the major issues for LEDs are wavelength instability, broad full width at half maximum (FWHM), and wide divergence angles. An unstable wavelength and broad FWHM may lead to color variations across the display, making the image appear less vibrant and less sharp. Furthermore, if the emission wavelength varies too much, it can cause issues with the viewing angle of the display because the light beams may not

be perceived as coming from a single point source as a result of spectral broadening. In addition, the quantum confined Stark effect (QCSE) is a phenomenon that mainly arises from the lattice mismatch within an InGaN/GaN quantum well [8]. The piezoelectric field induced by the lattice mismatch tilts the band edge, causing spatial separation of electrons and holes and thus reducing the electron-hole wavefunction overlap. Moreover, the lack of inversion symmetry in the c-plane Wurtzite material gives rise to an intrinsic spontaneous polarization, which enhances the QCSE [9]. The QCSE deteriorates the performance of micro-LEDs (μ -LEDs) by lowering efficiency, particularly in the green wavelengths (also known as the “green gap”), shifting the emission wavelength and limiting the bandwidth for communication [10]. In addition, as the indium content in the InGaN quantum well increases, the QCSE becomes more prominent, which further limits the efficiency of green μ -LEDs.

Recently, several solutions have been developed to alleviate the QCSE, such as using a strained-relaxed layer [8], a superlattice structure [11], a semipolar or nonpolar GaN substrate [12], or a staggered quantum well structure [13]. Among these solutions, the staggered quantum well structure is considered the most promising due to its ease of fabrication and ability to effectively increase the wavefunction overlap through band edge engineering [13]. In a typical staggered quantum well structure, the InGaN quantum wells are positioned in a “staggered” arrangement, which reduces the overall piezoelectric field in the quantum well and therefore suppresses the QCSE [13,14].

Resonant cavity light-emitting diodes (RCLEDs) have been proposed to resolve the issue of wide divergence angles in LEDs. The concept of RCLEDs is based on confining light within a resonant cavity to enhance the wavelength selectivity and decrease the divergence angle. This can be achieved by placing two distributed Bragg reflectors (DBRs) on both sides along the epitaxial direction. Each DBR consists of alternating layers of high and low refractive index materials, such as AlGaAs and GaAs. When the emission wavelength of the multiple quantum wells (MQWs) is precisely matched with the resonant wavelength of the Fabry–Pérot cavity, the light extraction efficiency can be greatly increased and the FWHM can be greatly reduced.

The first RCLED was proposed in 1994 by E. F. Schubert et al., where the DBRs were formed by InGaAs/GaAs with an emission wavelength of 930 nm [15]. Later, in 1999, Y.-K. Song et al. demonstrated the first InGaN-based RCLED, where the DBRs were formed by $\text{HfO}_2/\text{SiO}_2$ with an emission wavelength of 450 nm [16]. In 2006, R. H. Horng et al. reported a green InGaN-based RCLED with dielectric $\text{TiO}_2/\text{SiO}_2$ and silver mirrors, with an emission wavelength of 525 nm [17]. In 2022, S. Zhao et al. demonstrated an InGaN-based RCLED with single longitudinal-mode emission at 440 nm by using a $\text{Ta}_2\text{O}_5/\text{SiO}_2$ DBR-based filtering structure [18]. Finally, in 2022, K. B. Hong et al. proposed an InGaN-based photonic crystal LED (PCLED) with a nanoporous (NP) DBR as the bottom reflector and a strain-release layer [19].

In this paper, we first experimentally demonstrated a green InGaN-based c-plane μ -LED with a three-layer staggered quantum well structure and compared its optical and electrical properties to those of a commercial μ -LED. Then, we proposed and numerically analyzed a green InGaN-based micro-RCLED (μ -RCLED) with a three-layer staggered quantum well structure and a bottom NP DBR to address the issues of wavelength instability, broad FWHM, and large divergence angle. These designs are beneficial for developing μ -LED-based displays with high brightness, high contrast, and good color purity.

2. Experiments

In general, LEDs with smaller diameters or mesa sizes are beneficial for high-speed visible light communication and high-resolution display applications, because smaller LEDs can handle a higher current density with less self-heating effect [20]. In addition, minimizing the electrode size through the μ -LED architecture allows for low RC time constants. The design of a ring contact accompanied by a round mesa leads to better current spreading and electrical performance. Similarly, the sidewall defects due to the

etching process can be passivated by using atomic layer deposition (ALD), which further improves the light extraction efficiency.

The optical and electrical performance of μ -LEDs devices under direct current was measured using a spectrometer (Maya 2000 Pro), where the emitted light was collected by an integrating sphere. Figure 1 summarizes the electric performance of the $50\ \mu\text{m} \times 6\ \mu\text{m}$ μ -LED array with a three-layer staggered quantum well structure compared to that of a commercial $170\ \mu\text{m} \times 107\ \mu\text{m} \times 3\ \mu\text{m}$ μ -LED array. The detailed fabrication process of the $50\ \mu\text{m} \times 6\ \mu\text{m}$ μ -LED array in this work can be found in our previous research [8]. Figure 1a,c show the voltage as a function of current density for the commercial μ -LED and this work. Figure 1b,d show that the maximum EQE of the commercial μ -LED array is 18.9% before the efficiency droop at a low injection current. Moreover, the maximum EQE of the $50\ \mu\text{m} \times 6\ \mu\text{m}$ μ -LED array is 19.8% before the efficiency droop at a low injection current. However, the efficiency droop phenomenon occurs at low current density due to the QCSE in the polar c-plane GaN. Nevertheless, this device still suffers less efficiency droop compared to commercial c-plane wafers due to the presence of a three-layer staggered quantum well structure, which improves conversion efficiency at higher injection currents [13]. Furthermore, the power density of the $50\ \mu\text{m} \times 6\ \mu\text{m}$ μ -LED array in this work is also greater than that of the commercial μ -LED array.

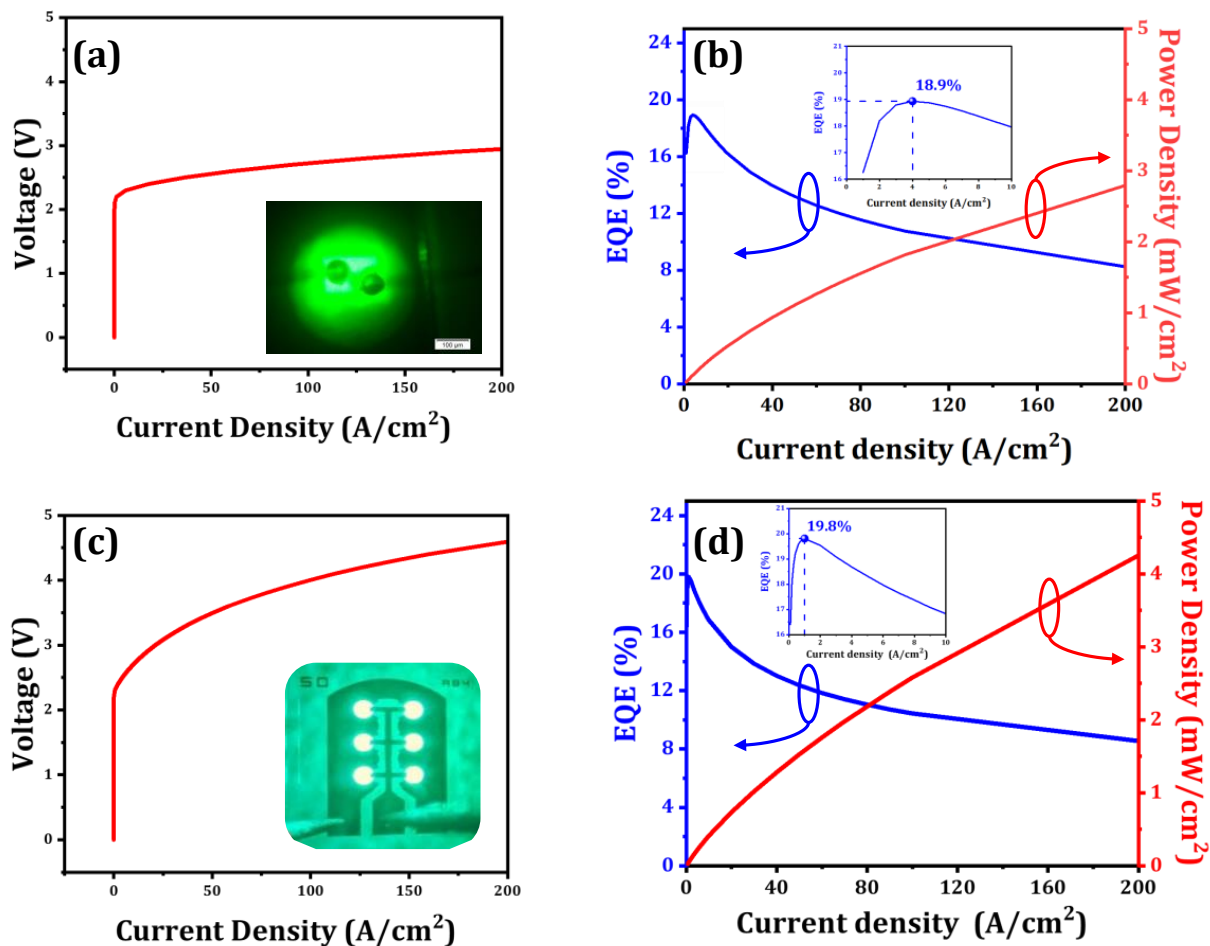


Figure 1. Measured (a) voltage and (b) external quantum efficiency and power density of the commercial green μ -LEDs with regular quantum wells as a function of current density, the inset is the optical microscopic view of the commercial μ -LED, where the scale is $100\ \mu\text{m}$. Measured (c) voltage and (d) external quantum efficiency and power density of μ -LEDs with staggered quantum wells as a function of current density, the inset is the optical microscopic view of the μ -LED in this work.

Figure 2 summarizes the optical performance of the $50 \mu\text{m} \times 6 \mu\text{m}$ -LED array and a commercial $170 \mu\text{m} \times 107 \mu\text{m} \times 3 \mu\text{m}$ -LED array. Figure 2a,c show the electroluminescence (EL) emission spectra for increasing injected current from 5 A/cm^2 to 200 A/cm^2 , showing the emission peak wavelength changing from 527 nm to 508.6 nm and 508.8 nm to 498.3 nm for the commercial $\mu\text{-LED}$ and this work, respectively, in the green spectral region. Moreover, the peak wavelength shift is 18.4 nm and 10.5 nm for the commercial and this work, respectively, as shown in Figure 2b,d. Both the wavelength shift and FWHM of this work show better performance than the commercial $\mu\text{-LED}$ due to the bandgap engineering of the staggered quantum well structure.

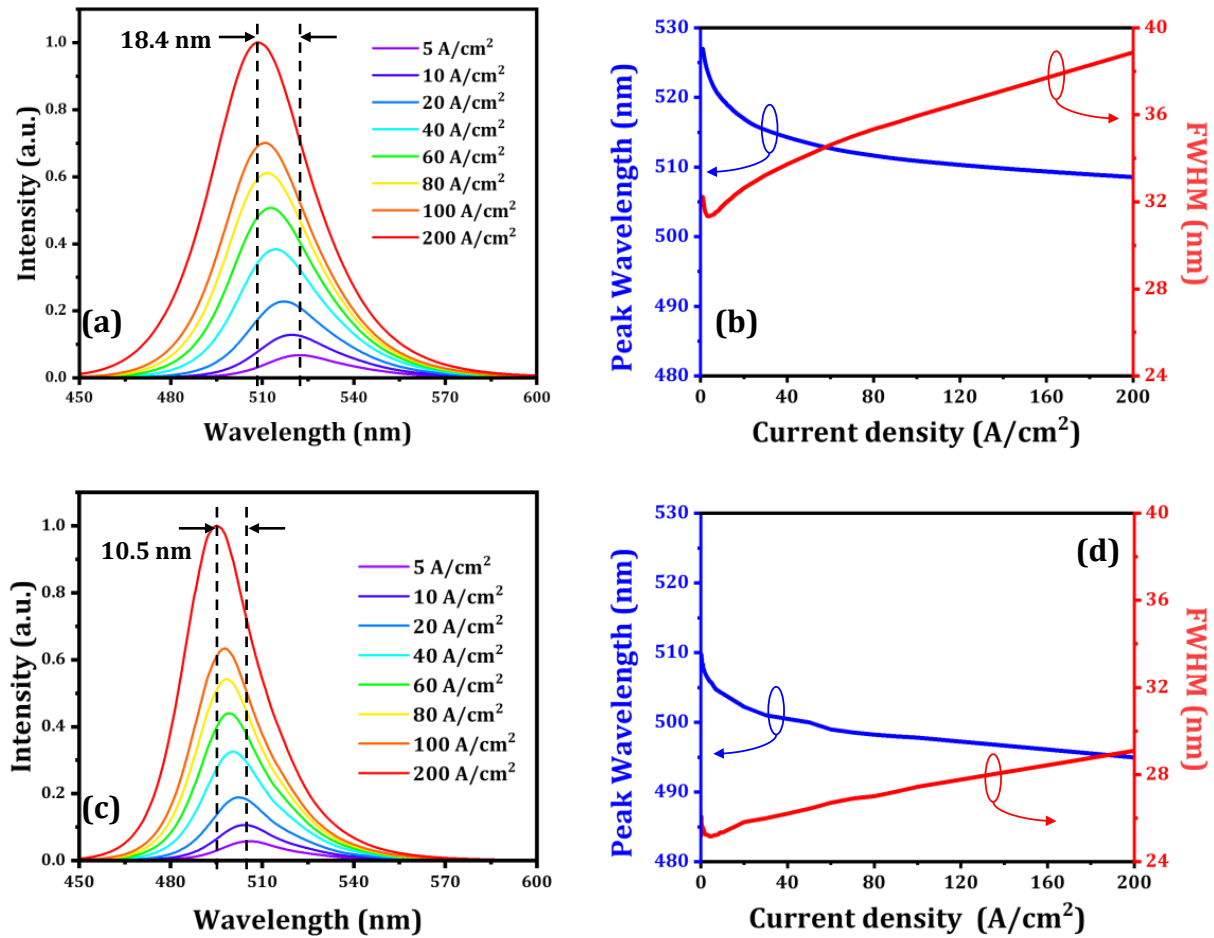


Figure 2. Measured (a) emission spectra and (b) wavelength shifts and FWHMs of the commercial green $\mu\text{-LED}$ s with regular quantum wells. Measured (c) emission spectra and (d) wavelength shifts and FWHMs of $\mu\text{-LED}$ s with staggered quantum wells.

Figure 3 summarizes the temperature-dependent wavelength as a function of current density. Under the same current density, the wavelengths of both $\mu\text{-LED}$ s exhibit a red shift as the temperature increases. At 200 A/cm^2 , the redshift is 4.18 nm and 3.52 nm from 313 K to 373 K for the commercial $\mu\text{-LED}$ and the $\mu\text{-LED}$ from this work, respectively. The red shift in the wavelength is primarily caused by bandgap shrinkage due to heating [21,22]. Furthermore, the difference in redshift may be attributed to the thermal resistance of the $\mu\text{-LED}$ s, which is caused by variations in the epitaxial structure and packaging.

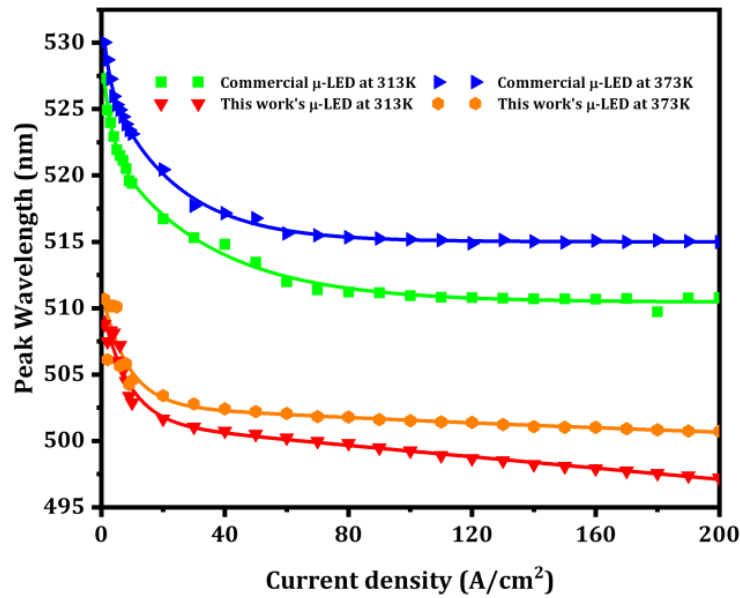


Figure 3. Measured temperature-dependent wavelength as a function of current density.

To further investigate the effect of self-heating in μ -LEDs more thoroughly, the optical performance of both commercial μ -LEDs and μ -LEDs from this study was measured under different duty cycles (DC). The μ -LEDs were driven by a pulse current source (LDP-3811) with a pulse width of 100 μ s at duty cycles of 5% and 50%. The emitted light was then collected by a photodiode energy meter (PD10-C). The results are illustrated in Figure 4. Under pulse mode operation at the same current density, the results reveal that both the commercial μ -LEDs and the μ -LEDs from this work exhibit superior energy density at a duty cycle of 5% compared to a duty cycle of 50%, due to more effective thermal management, reduced thermal stress, resulting in improved efficiency, higher peak power, and decreased device degradation [20,23,24]. This emphasizes the importance of carefully selecting the appropriate duty cycle for pulse mode operation to maximize energy density and minimize self-heating, ultimately enhancing the performance and longevity of LED devices across various applications.

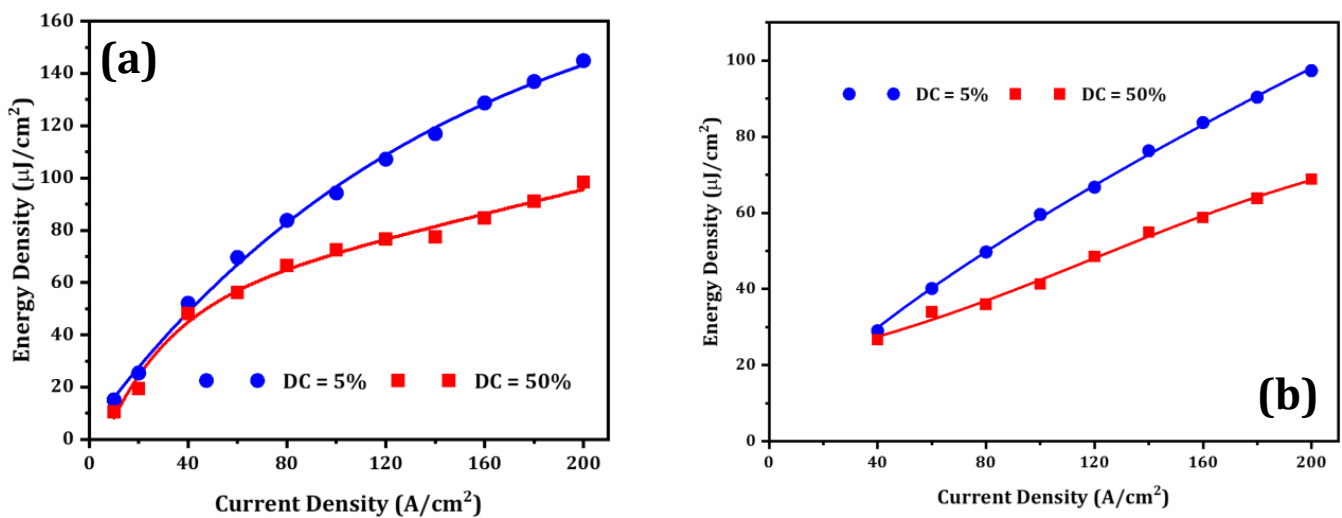


Figure 4. Measures optical energy density at different duty cycles (DC) for (a) commercial μ -LEDs and (b) μ -LED from this work.

3. Simulated Method and Structure Definition

In this study, systematic numerical studies have been performed by using the commercial semiconductor device simulation tool Crosslight. The settings of perfectly matched layers (PML) at the lateral and bottom surfaces of the μ -RCLED were the critical boundary conditions. A monitor for the far-field calculation was also set on top of the LED. The three-dimensional (3D) schematic diagram of the proposed μ -RCLED is shown in Figure 5. The epitaxial structure is composed of an undoped GaN layer, 11.5 pairs of GaN/NP-n-GaN DBRs, an n-GaN layer, three pairs of InGaN/GaN MQWs as the active region, a 100 nm p-GaN layer, a 100 nm indium tin oxide (ITO) thin film as a current-spreading layer, and 6.5 pairs of Ta₂O₅/SiO₂ DBRs. To mitigate the QCSE, the staggered MQW structure was applied in our design. The symmetric staggered InGaN MQWs are established by three layers of In_{0.155}Ga_{0.845}N (0.7 nm)/In_{0.335}Ga_{0.665}N (2.1 nm)/In_{0.155}Ga_{0.845}N (0.7 nm) and the GaN barrier is 13 nm. In comparison, the regular MQWs are composed of 3.5 nm In_{0.27}Ga_{0.73}N QWs and a 13 nm GaN barrier. Both types of InGaN quantum wells have an emission wavelength of 525 nm. Moreover, the strain-relaxation of the active region is accomplished by means of the epitaxial NP n-GaN DBR [12]. To eliminate the random nature of the pores distributed in NP-GaN DBR, which raises questions regarding the reliability of the simulation, in this work, we aimed to achieve results that are independent of the simulation region size. Therefore, we set the NP-DBR as a bulk material with a given refractive index, thus eliminating the influence of the simulation region size. The refractive index of the NP-GaN DBR was estimated using the following Equation (1) [25–27]:

$$\text{Porosity (\%)} = \left(1 - \frac{n_{\text{NP-GaN}}}{n_{\text{GaN}}} \right) \quad (1)$$

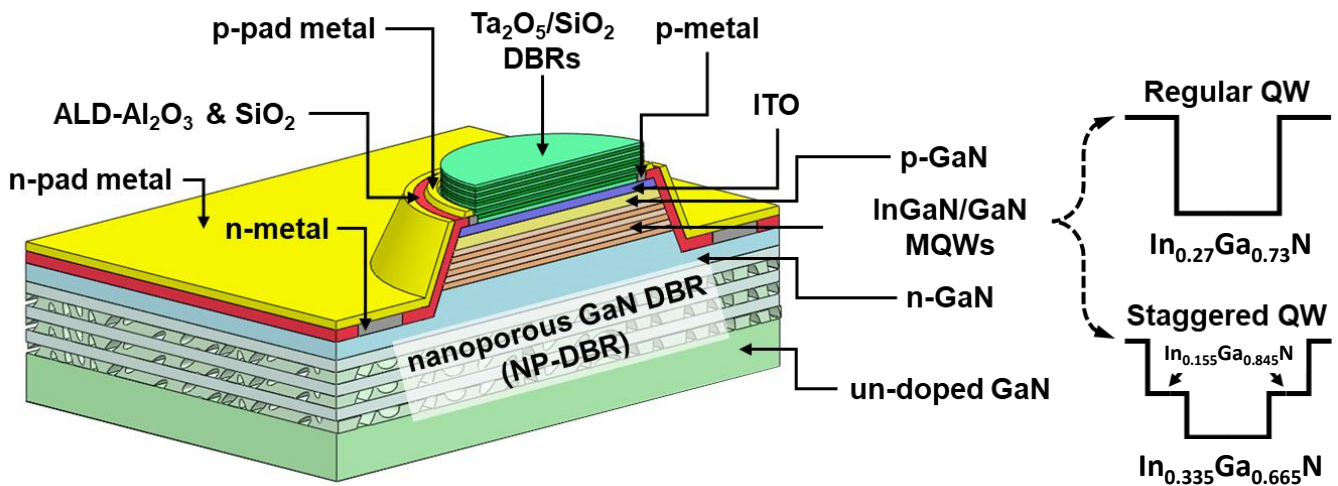


Figure 5. 3D schematic of the InGaN-based green μ -RCLED with regular or staggered MQWs. The mesa diameter and the total height of the μ -RCLEDs are 50 μm and 1 μm , respectively.

A potential fabrication process for the μ -RCLED is as follows: The nanoporous n-GaN layer can be created through the following chemical etching process, which involved making indium contacts on the n-GaN layer, immersing the n-GaN and platinum targets into a nitride acid solution, applying a forward voltage, and then rinsing the finished product in deionized water followed by blowing with N₂ to dry. An ITO layer can be deposited on the p-GaN surface using RF sputtering or electron beam evaporation, and the fabrication of Ta₂O₅/SiO₂ multilayers can be prepared by plasma-enhanced chemical vapor deposition (PECVD). In addition, μ -LEDs with an arbitrary diameter can be defined through a photolithography process. The mesa depth of 1 μm can be etched by using a HCl solution for ITO and ICP-RIE for GaN. A Ti/Al/Ni/Au layer can be deposited as the

electrodes, and a 5 nm-thick aluminum oxide (Al_2O_3) passivation layer can be grown on the full wafer to reduce sidewall defects generated by mesa etching. Then, a 200 nm SiO_2 layer can be deposited to cover the Al_2O_3 layer. Finally, the metal contacts can be connected to the p-metal and n-type contact layer to complete the manufacture of the μ -RCLED device.

4. Result and Discussion

4.1. Wavefunction Overlap and Peak Wavelength Shift

An enhancement of the internal quantum efficiency (IQE) can be achieved by increasing the radiative recombination rate. The recombination rate $W_{\text{spontaneous}}$ can be expressed as follows: $W_{\text{spontaneous}} \sim |\langle u_c | u_v \rangle|^2 \cdot |\Gamma_{e-hh}|^2$ [28], where $|u_c\rangle$ and $|u_v\rangle$ are the Bloch envelope functions for the conduction and valence bands, respectively, and $|\Gamma_{e-hh}|$ is the electron and hole wavefunction overlap integral. The energy band diagrams and the wavefunction overlaps of the regular and staggered quantum wells at the input current equal to 300 mA are shown in Figure 6. In Figure 6a, the regular InGaN quantum well displays a large spatial separation between electron and hole wavefunction due to an internal electric field, with the electron-hole wavefunction overlap $\Gamma_{e-hh} = 8.8\%$. In Figure 6b, a three-layer staggered InGaN quantum well is shown, where a higher indium content sublayer in the center, sandwiched between two sublayers with lower indium content, draws both electron and hole wavefunctions to the center, resulting in the significantly improved wavefunction overlap $\Gamma_{e-hh} = 18.1\%$. By optimizing the indium contents and thicknesses of the sublayers in the staggered InGaN quantum well, the electron-hole wavefunction overlap can be increased by more than two times, compared to the regular InGaN quantum well.

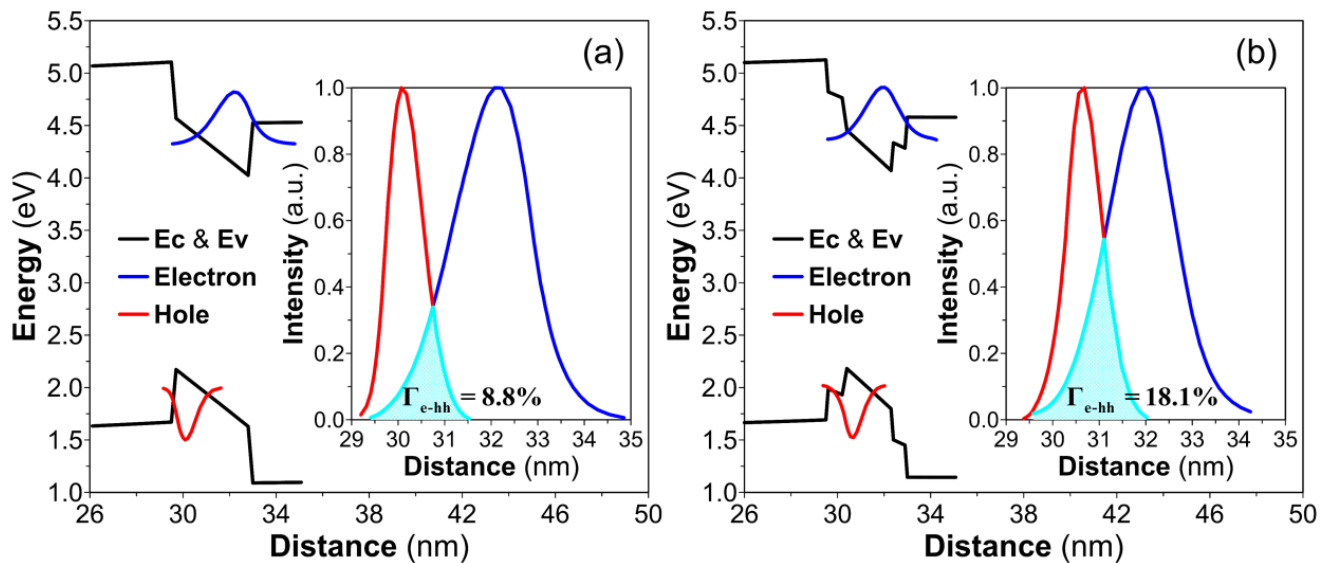


Figure 6. Energy band diagrams and wavefunctions of (a) regular and (b) staggered quantum wells with the input current equal to 300 mA. The zoom-in images of electron and hole wavefunctions for both kinds of quantum wells are plotted in the insets. Here Γ_{e-hh} represents the integral overlap of electron and hole wavefunctions.

Figure 7 summarizes the optical performance of the regular and staggered quantum wells. Figure 7a,b show the electroluminescence spectra of ordinary μ -LEDs with regular MQWs. When the input current increases from 30 mA to 300 mA, the peak wavelength changes from 525.50 nm to 515.25 nm, corresponding to a blue-shift of 10.25 nm, and the FWHM increases from 32 nm to 39 nm. In contrast, Figure 7c,d show the electroluminescence spectra of μ -LEDs with staggered MQWs. When the input current increases from 30 mA to 300 mA, the peak wavelength has a relatively small blue-shift from 527.25 nm to 525.00 nm and the FWHM increases from 29.5 nm to 34.5 nm. Here the broad FWHM of 34.5 nm is problematic for color purity, as high color purity is accompanied by narrow

FWHM. Both the commercial and staggered quantum well μ -LEDs show better performance than the ones demonstrated in Section 3 due to the presence of the NP DBR as the strain-released layer, which mitigates the effect of the QCSE.

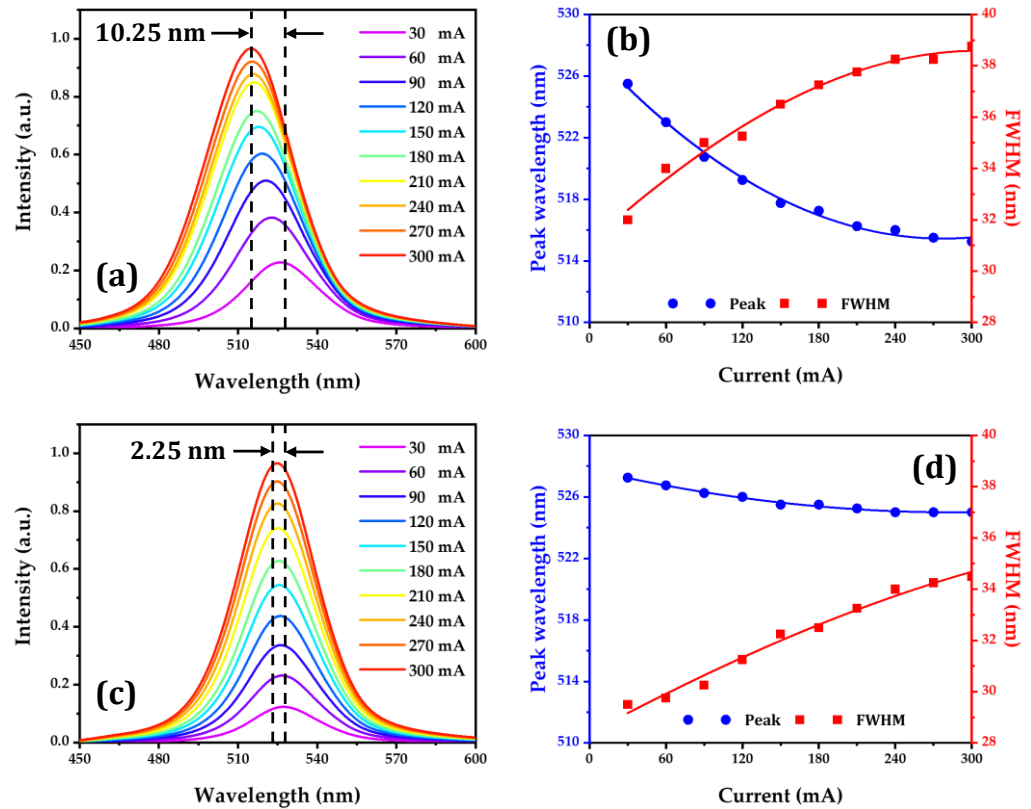


Figure 7. (a,b) Electroluminescence spectra, peak wavelength shifts, and FWHMs of the μ -LEDs with regular MQWs. (c,d) Electroluminescence spectra, peak wavelength shifts, and FWHMs of the μ -LEDs with staggered MQWs.

4.2. Reflectivity Spectrum and FWHM

To resolve the issue of broad FWHM at high input current, a Fabry–Pérot cavity comprising a GaN layer, an NP-n-GaN DBR, and different pairs of Ta₂O₅/SiO₂ DBRs is added. The 11.5 pairs of NP-n-GaN DBRs were successfully fabricated and the optical reflectivity was measured in our previous work [8]. Based on our previous experimental result, a porosity of 35.7% in the NP-n-GaN layer is assumed, and the resulting reflectivity at 525 nm is 96.7%. In addition, the reflectivity spectra with different numbers of Ta₂O₅/SiO₂ DBR pairs are shown in Figure 8a, and the maximum reflectivity at 525 nm is 97.9% with 6.5 Ta₂O₅/SiO₂ DBR pairs. As we know that the FWHM of an Airy distribution in the frequency domain for a simple Fabry–Pérot cavity consisting of two opposite planar mirrors can be expressed as follows: $\text{FWHM} = (c/2 \cdot n \cdot \pi \cdot L)(1-R_1 \cdot R_2)(R_1 \cdot R_2)^{1/2}$ [29], where c , L , n , R_1 , and R_2 represent the speed of light in vacuum, cavity length, the reflectivity of cavity material, and optical reflectivities for the top and bottom mirrors, respectively. Based on the above equation, if R_1 and R_2 approach unity, $1-R_1 \cdot R_2$ approaches zero and thus the FWHM approaches zero. Here the simulated FWHMs for different numbers of Ta₂O₅/SiO₂ DBR pairs are shown in Figure 8b, demonstrating that the FWHM indeed decreases as the reflectivity increases. The FWHMs for 5.5 and 6.5 pairs of DBRs are 0.315 nm and 0.294 nm, respectively. When the number of DBR pairs is larger than 6.5, the FWHM gradually saturates. Moreover, since the output power of the μ -RCLD will reach its maximum when the reflectivity of the top Ta₂O₅/SiO₂ DBR is closest to that of the bottom NP DBR [18], the 6.5 pairs of Ta₂O₅/SiO₂ DBRs represent the best design in this work.

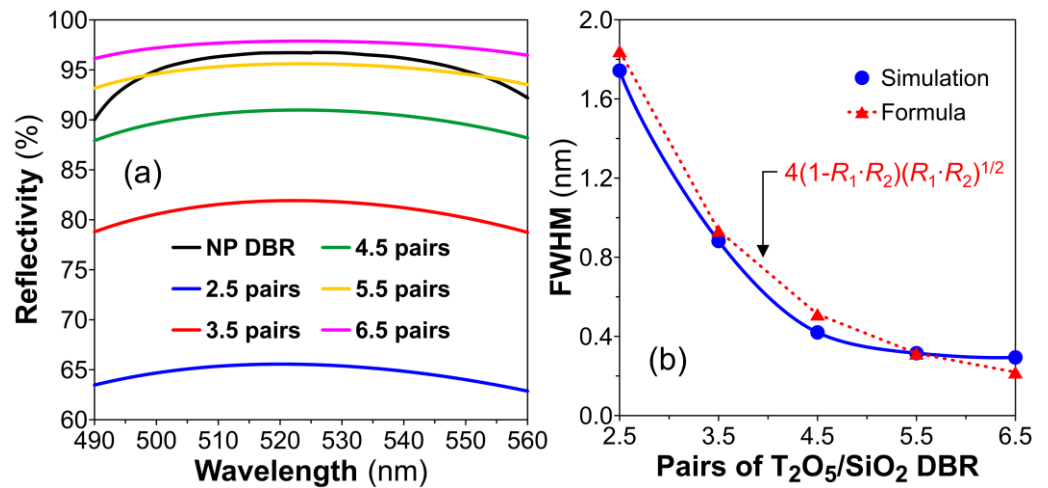


Figure 8. (a) Reflectivity spectra of the top reflective mirror with different pairs of Ta₂O₅/SiO₂ DBRs. The optical reflectivity of 11.5 pairs of GaN/NP-n-GaN DBR was plotted by the black line. (b) FWHMs with different numbers of Ta₂O₅/SiO₂ DBR pairs.

4.3. Emission Spectrum of μ -RCLED

Based on the discussion above, the design of staggered MQWs can substantially alleviate the blue-shift issue induced by the QCSE. Additionally, by applying a high-quality resonant cavity, the FWHM can also be reduced. The RCLED is similar to a Fabry–Pérot cavity, and the longitudinal mode spacing can be expressed as $\Delta\lambda \equiv \lambda^2 / (2n_g L_{\text{eff}})$, where n_g ($n_g = 2.6$ in the calculation for the target wavelength of 525 nm) and L_{eff} are the group index and effective cavity length, respectively. Based on this definition, the mode spacing shrinks with the cavity length. If the longitudinal mode spacing is set to be 20 nm, then the effective cavity length of the RCLED should be approximately 2.65 μm , indicating that $L_{\text{eff}} = 5\lambda$ for achieving a green RCLED with high-quality-factor and stable single-mode emission. Meanwhile, the total resonant mode loss of a Fabry–Pérot cavity can be calculated by the following equation: $\alpha_i + \alpha_m = 2 \cdot n_g \cdot \pi / (\lambda \cdot Q)$ and $\alpha_m = -1 / (2 \cdot L_{\text{eff}}) \ln(R_1 \cdot R_2)$ [30,31]. Here α_i , α_m , and Q are the internal (material) loss, mirror loss, and cavity quality factor, respectively. Consequently, the Q factor is inversely dependent on the effective cavity length and the product of R_1 and R_2 . The current-dependent emission spectra of the InGaN-based green μ -RCLEDs with the regular and staggered MQWs are shown in Figure 9a,b. The electroluminescence spectra for the green μ -RCLEDs with both kinds of InGaN MQWs possess generic Airy-distribution-like peaks. Regardless of the InGaN quantum well structure, the central peak wavelength is located at 525 nm. In addition, as the input current increases from 30 mA to 300 mA, the emission wavelength remains almost unchanged, and the adjacent second-highest peak at a wavelength of 505 nm becomes more obvious. The wavelength difference is due to the longitudinal mode spacing. The output power of the μ -RCLEDs with regular and staggered MQWs with different input currents is shown in Figure 9c. The output power of the green μ -RCLED with staggered MQWs increases steadily as the current increases, due to the greater wavelength stability. In contrast, the output power of the μ -RCLED drops as the input current exceeds 240 mA.

4.4. Divergence Angle of μ -RCLED with Staggered MQWs

We have also investigated the far-field emission patterns of the μ -RCLED with staggered MQWs for increasing numbers of Ta₂O₅/SiO₂ DBR pairs from 2.5 to 6.5, as shown in Figure 10. The calculated radiation profiles for different pairs of Ta₂O₅/SiO₂ DBRs are all narrower than the Lambertian-like distribution of conventional LEDs, as plotted by the blue line in Figure 10a. The calculated divergence angle decreases from 71.5° to 56.4° as the number of Ta₂O₅/SiO₂ DBR pairs increases from 2.5 to 6.5, as shown in Figure 10b.

The angular color shifts within $\pm 30^\circ$ are achieved to improve the light extraction efficiency when the number of DBR pairs is equal to or larger than 5.5.

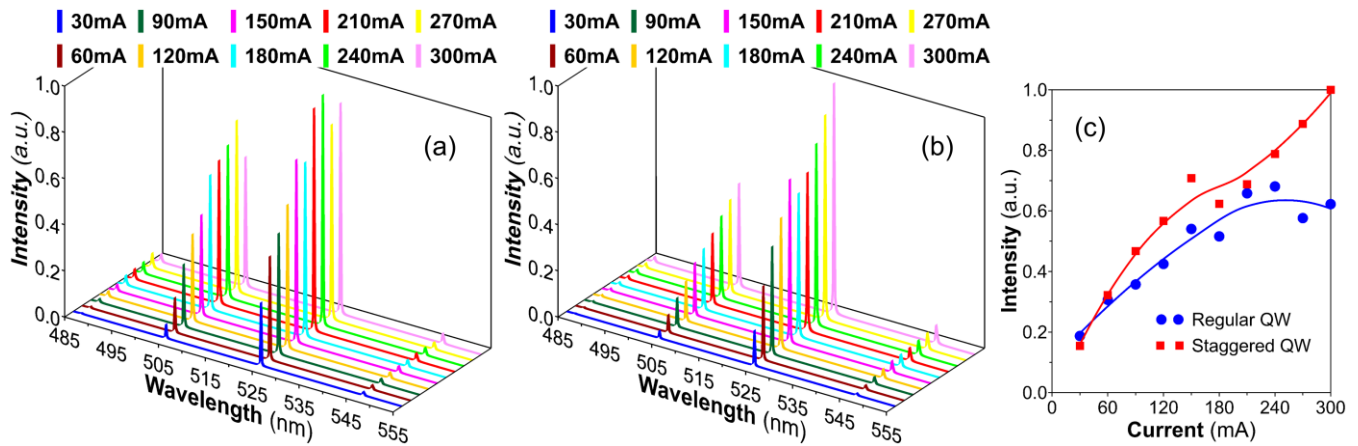


Figure 9. Electroluminescence spectra of the green μ -RCLDs with (a) regular and (b) staggered MQWs. (c) Output power as a function of the input current for the two μ -RCLDs.

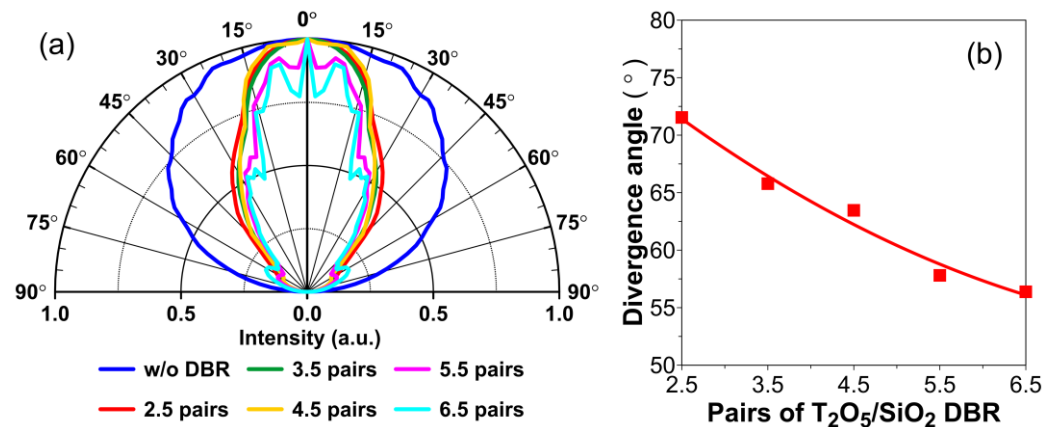


Figure 10. (a) Far-field emission patterns of the green μ -RCLDs with staggered MQWs operating at 300 mA for different pairs of $\text{Ta}_2\text{O}_5/\text{SiO}_2$ DBRs. The blue line indicates the emission pattern of conventional LEDs. (b) Far-field divergence angle as a function of pairs of DBRs.

5. Conclusions

We have experimentally demonstrated a green InGaN-based c-plane μ -LED with a three-layer staggered quantum well structure and compared its optical and electrical properties to those of a commercial μ -LED. We then numerically investigated the optoelectronic characteristics of an InGaN-based green μ -RCLD consisting of 11.5 pairs of nanoporous n-GaN DBRs with 35.7% of air-void at the bottom and 6.5 pairs of $\text{Ta}_2\text{O}_5/\text{SiO}_2$ DBRs at the top. The InGaN MQW structure emitting at a wavelength of 525 nm serves as the active region. A three-layer symmetric staggered MQW structure is adopted in our design to deal with the issue of wavelength instability. Meanwhile, the dependence of the number of $\text{Ta}_2\text{O}_5/\text{SiO}_2$ DBR pairs on the FWHM, optical power output, and far-field divergence angle is also studied. By optimizing the indium content and thickness of the sublayers in the staggered InGaN MQWs, the electron-hole wavefunction overlap can be increased by more than two times, compared to the regular MQWs. The numerical results indicate that the wavefunction overlaps are 8.8% and 18.1% for the regular and staggered MQWs, respectively. Furthermore, the blue-shift of electroluminescence, as the input current increases from 30 mA to 300 mA, is reduced from 10.25 nm for the regular MQWs to 2.25 nm for the staggered MQWs. When 6.5 pairs of $\text{Ta}_2\text{O}_5/\text{SiO}_2$ DBRs are applied on top, the FWHM can

be reduced from 35–40 nm obtained with the ordinary μ -LED to about 0.3 nm obtained with the μ -RCLED. Due to the narrow FWHM and the small blue-shift of electroluminescence, the μ -RCLED with staggered MQWs can maintain high output power even at high input currents. In contrast, the output power with regular MQWs drops when the input current exceeds 240 mA. The far field divergence angle drops from 71.5° to 56.4° as the number of $\text{Ta}_2\text{O}_5/\text{SiO}_2$ DBR pairs increases from 2.5 to 6.5. In summary, our simulation results demonstrate that the proposed designs for green μ -RCLEDs to achieve high wavelength stability and narrow FWHM may pave the way for developing next-generation light sources.

Author Contributions: Conceptualization, H.-C.K.; methodology, K.-B.H. and W.-T.H.; software, W.-T.H. and Y.-H.B.; validation, K.-B.H., W.-T.H. and Y.-H.B.; investigation, K.-B.H., Y.-H.P., W.-T.H. and H.-C.K.; writing—original draft preparation, K.-B.H., C.-C.T., T.-H.H. and W.-T.H.; writing—review and editing, K.-B.H., C.-C.T., T.-H.H., T.-Y.L. and W.-T.H. and H.-C.K.; supervision, C.-H.H., Y.L. and H.-C.K. All authors have read and agreed to the published version of the manuscript.

Funding: This research was funded by the Ministry of Science and Technology in Taiwan (Grant Nos. MOST 110-2622-8-A49-008-SB, 111-2124-M-A49-004-, 111-2622-E-A49-014-).

Institutional Review Board Statement: Not applicable.

Informed Consent Statement: Not applicable.

Data Availability Statement: Not applicable.

Acknowledgments: The authors express their gratitude to the Innolux corporation and Hon Hai Research Institute for their technical support and helpful discussion.

Conflicts of Interest: The authors declare no conflict of interest.

References

1. Chou, H.-H.; Huang, W.-T. Asymmetrical bidirectional optical wireless communication system based on a transmissive 1D LC-SLM for NG-PON2. *Opt. Lett.* **2020**, *45*, 4543–4546. [[CrossRef](#)]
2. Chou, H.H.; Huang, W.T. Wavelength Tunable Asymmetric B-OWC System Based on Self-Injection Locking for TDM-PONs. *IEEE Photonics Technol. Lett.* **2021**, *33*, 370–372. [[CrossRef](#)]
3. Li, C.; Lu, H.; Tsai, W.; Wang, Z.; Hung, C.; Su, C.; Lu, Y. A 5 m/25 Gbps Underwater Wireless Optical Communication System. *IEEE Photonics J.* **2018**, *10*, 1–9. [[CrossRef](#)]
4. Wu, T.; Yue, L.; Huang, Y.-M.; Liu, M.; James Singh, K.; Lin, W.; Lu, T.; Zheng, X.; Zhou, Z.; Kuo, H.-C.; et al. A highly stable full-color display device with VLC application potential using semipolar micro-LEDs and all-inorganic encapsulated perovskite nanocrystal. *Photon. Res.* **2021**, *9*, 2132. [[CrossRef](#)]
5. Do, T.-H.; Yoo, M. An in-Depth Survey of Visible Light Communication Based Positioning Systems. *Sensors* **2016**, *16*, 678. [[CrossRef](#)] [[PubMed](#)]
6. Yu, T.-C.; Huang, W.-T.; Lee, W.-B.; Chow, C.-W.; Chang, S.-W.; Kuo, H.-C. Visible Light Communication System Technology Review: Devices, Architectures, and Applications. *Crystals* **2021**, *11*, 1098. [[CrossRef](#)]
7. Peng, C.-Y.; Huang, W.-T.; Lu, Z.-K.; Chen, S.-C.; Kuo, H.-C. Design of High-Power Red VCSEL on a Removable Substrate. *Photonics* **2022**, *9*, 763. [[CrossRef](#)]
8. Huang, W.-T.; Peng, C.-Y.; Chiang, H.; Huang, Y.-M.; Singh, K.J.; Lee, W.-B.; Chow, C.-W.; Chen, S.-C.; Kuo, H.-C. Toward high-bandwidth yellow-green micro-LEDs utilizing nanoporous distributed Bragg reflectors for visible light communication. *Photon. Res.* **2022**, *10*, 1810–1818. [[CrossRef](#)]
9. Takeuchi, T.; Amano, H.; Akasaki, I. Theoretical Study of Orientation Dependence of Piezoelectric Effects in Wurtzite Strained GaInN/GaN Heterostructures and Quantum Wells. *Jpn. J. Appl. Phys.* **2000**, *39*, 413. [[CrossRef](#)]
10. Piprek, J. Efficiency droop in nitride-based light-emitting diodes. *Phys. Status Solidi A* **2010**, *207*, 2217–2225. [[CrossRef](#)]
11. Huang, Y.-M.; Peng, C.-Y.; Miao, W.-C.; Chiang, H.; Lee, T.-Y.; Chang, Y.-H.; Singh, K.J.; Iida, Z.D.; Horng, R.-H.; Chow, C.-W.; et al. High-efficiency InGaN red micro-LEDs for visible light communication. *Photon. Res.* **2022**, *10*, 1978–1986. [[CrossRef](#)]
12. Chen, S.-W.H.; Huang, Y.-M.; Chang, Y.-H.; Lin, Y.; Liou, F.-J.; Hsu, Y.-C.; Song, J.; Choi, J.; Chow, C.-W.; Lin, C.-C.; et al. High-Bandwidth Green Semipolar (20–21) InGaN/GaN Micro Light-Emitting Diodes for Visible Light Communication. *ACS Photonics* **2020**, *7*, 2228–2235. [[CrossRef](#)]
13. Arif, R.A.; Ee, Y.-K.; Tansu, N. Polarization engineering via staggered InGaN quantum wells for radiative efficiency enhancement of light emitting diodes. *Appl. Phys. Lett.* **2007**, *91*, 091110. [[CrossRef](#)]
14. Zhao, H.; Arif, R.A.; Tansu, N. Design Analysis of Staggered InGaN Quantum Wells Light-Emitting Diodes at 500–540 nm. *IEEE J. Sel. Top. Quantum Electron.* **2009**, *15*, 1104–1114. [[CrossRef](#)]

15. Schubert, E.F.; Hunt, N.E.J.; Micovic, M.; Malik, R.J.; Sivco, D.L.; Cho, A.Y.; Zyzdik, G.J. Highly Efficient Light-Emitting Diodes with Microcavities. *Science* **1994**, *265*, 943–945. [[CrossRef](#)]
16. Song, Y.-K.; Diagne, M.; Zhou, H.; Nurmikko, A.V.; Carter-Coman, C.; Kern, R.S.; Kish, F.A.; Krames, M.R. A vertical injection blue light emitting diode in substrate separated InGaN heterostructures. *Appl. Phys. Lett.* **1999**, *74*, 3720–3722. [[CrossRef](#)]
17. Horng, R.H.; Wei-Kai, W.; Shin-Yung, H.; Dong-Sing, W. Effect of resonant cavity in wafer-bonded Green InGaN LED with dielectric and silver mirrors. *IEEE Photonics Technol. Lett.* **2006**, *18*, 457–459. [[CrossRef](#)]
18. Zhao, S.; Xu, B.; Zhao, Z.; Gu, D.; Zhang, Y.; Lv, W.; Lv, X. Gallium nitride-based resonant cavity light-emitting diode with single-longitudinal-mode emission. *Opt. Lett.* **2022**, *47*, 4616–4619. [[CrossRef](#)]
19. Hong, K.-B.; Huang, W.-T.; Hsu, W.-C.; Tu, C.-C.; Kuo, H.-C. Investigation of InGaN-Based Green Micro-Photonic-Crystal-Light-Emitting-Diodes with Bottom, Nanoporous, Distributed Bragg Reflectors. *Photonics* **2022**, *9*, 939. [[CrossRef](#)]
20. Gong, Z.; Jin, S.; Chen, Y.; McKendry, J.; Massoubre, D.; Watson, I.M.; Gu, E.; Dawson, M.D. Size-dependent light output, spectral shift, and self-heating of 400 nm InGaN light-emitting diodes. *J. Appl. Phys.* **2010**, *107*, 013103. [[CrossRef](#)]
21. Sarkar, N.; Ghosh, S. Temperature dependent band gap shrinkage in GaN: Role of electron–phonon interaction. *Solid State Commun.* **2009**, *149*, 1288–1291. [[CrossRef](#)]
22. Auvergne, D.; Camassel, J.; Mathieu, H. Band-gap shrinkage of semiconductors. *Phys. Rev. B* **1975**, *11*, 2251–2259. [[CrossRef](#)]
23. Haemmer, M.; Roycroft, B.; Akhter, M.; Dinh, D.V.; Quan, Z.; Zhao, J.; Parbrook, P.J.; Corbett, B. Size-Dependent Bandwidth of Semipolar (11-22) Light-Emitting-Diodes. *IEEE Photonics Technol. Lett.* **2018**, *30*, 439–442. [[CrossRef](#)]
24. Tian, P.; McKendry, J.J.D.; Gong, Z.; Guilhabert, B.; Watson, I.M.; Gu, E.; Chen, Z.; Zhang, G.; Dawson, M.D. Size-dependent efficiency and efficiency droop of blue InGaN micro-light emitting diodes. *Appl. Phys. Lett.* **2012**, *101*, 231110. [[CrossRef](#)]
25. Lee, K.J.; Oh, S.; Kim, S.-J.; Yim, S.-Y.; Myoung, N.; Lee, K.; Kim, J.S.; Jung, S.H.; Chung, T.-H.; Park, S.-J. Enhanced optical output in InGaN/GaN light-emitting diodes by tailored refractive index of nanoporous GaN. *Nanotechnology* **2019**, *30*, 415301. [[CrossRef](#)] [[PubMed](#)]
26. Yoldas, B.E.; Partlow, D.P. Formation of broad band antireflective coatings on fused silica for high power laser applications. *Thin Solid Film.* **1985**, *129*, 1–14. [[CrossRef](#)]
27. Mao, P.; Sun, F.; Yao, H.; Chen, J.; Zhao, B.; Xie, B.; Han, M.; Wang, G. Extraction of light trapped due to total internal reflection using porous high refractive index nanoparticle films. *Nanoscale* **2014**, *6*, 8177–8184. [[CrossRef](#)]
28. Arif, R.A.; Zhao, H.; Ee, Y.K.; Tansu, N. Spontaneous Emission and Characteristics of Staggered InGaN Quantum-Well Light-Emitting Diodes. *IEEE J. Quantum Electron.* **2008**, *44*, 573–580. [[CrossRef](#)]
29. Stacy, W.; Mueller, G.; Reitze, D.; Tanner, D.B.; Whiting, B.F. Linewidth-broadened Fabry–Perot cavities within future gravitational wave detectors. *Class. Quantum Gravity* **2004**, *21*, S1031. [[CrossRef](#)]
30. Butté, R.; Christmann, G.; Feltin, E.; Castiglia, A.; Levrat, J.; Cosendey, G.; Altoukhov, A.; Carlin, J.-F.; Grandjean, N. *Room Temperature Polariton Lasing in III-Nitride Microcavities: A Comparison with Blue GaN-Based Vertical Cavity Surface Emitting Lasers*; SPIE: Washington, DC, USA, 2009; Volume 7216.
31. Zhao, G.Y.; Ishikawa, H.; Yu, G.; Egawa, T.; Watanabe, J.; Soga, T.; Jimbo, T.; Umeno, M. Thermo-optical nonlinearity of GaN grown by metalorganic chemical- vapor deposition. *Appl. Phys. Lett.* **1998**, *73*, 22–24. [[CrossRef](#)]

Disclaimer/Publisher’s Note: The statements, opinions and data contained in all publications are solely those of the individual author(s) and contributor(s) and not of MDPI and/or the editor(s). MDPI and/or the editor(s) disclaim responsibility for any injury to people or property resulting from any ideas, methods, instructions or products referred to in the content.